Atomistic details of precipitates in lean Al-Mg-Si alloys with trace additions of Ag and Ge studied by HAADF-STEM and DFT

Eva A. Mørtsell*[1], Sigmund J. Andersen[2], Jesper Friis[2], Calin D. Marioara[2] and Randi Holmestad[1]

[1]*Department of Physics, Norwegian University of Science and Technology (NTNU), 7491 Trondheim, Norway*

[2]*SINTEF Materials and Chemistry, N-7465 Trondheim, Norway*

*Corresponding author. E-mail address: eva.mortsell@ntnu.no

Atomistic details of precipitates in lean Al-Mg-Si alloys with trace additions of Ag and Ge studied by HAADF-STEM and DFT

Bonding energies and volume misfits for alloying elements and vacancies in multi-component Al-Mg-Si alloys have been calculated using density functional theory and the results have been compared with numbers obtained by atomic scale precipitate structure analysis, using high angle annular dark-field scanning transmission electron microscopy. The techniques in combination provide new insight into precipitation in these alloys. In the Ge containing alloy were found two new stacking configurations of the well-known strengthening phase β''. In the alloy with Ag a new Q'/C - like local configuration containing Ag was discovered, and a model has been proposed. The experimental results are justified by simulations.

Keywords: aluminium alloys; HAADF-STEM; density-functional theory; Si/Ge; nanosized precipitates; crystal structure

1 Introduction

The current focus on environmental-friendly materials underlines the increasingly important role light metals will have to play. Aluminium alloys are light but at the same time strong, and when the products have served their purpose they can be recycled using just a fraction of the initial energy costs. They can be tailored-made with desirable combinations of material properties such as corrosion resistance, formability and ductility, which lead to reduced material usage, lower costs and longer life.

Aluminium 6xxx alloys are shaped by extrusion or rolling into products. A final ageing heat treatment hardens the products, creating nanosized semi-coherent, needle-shaped precipitates to form from the alloying elements. The precipitate needles obstruct dislocations, consequently increasing the material strength. The needles in 6xxx alloys mainly consist of Mg and Si in addition to Al itself [1] [2] [3], but other added elements may enter the precipitates as well. Elements like Li, Cu, Zn, Ag and Ge have proven to be beneficial for the nucleation and growth of precipitates, and they have consequently been added in multiple

combinations and amounts [4] [5] [6] [7] [8]. It is beneficial for the extrusion and rolling processes to keep the alloys as lean as possible. Thus, we need to know how small (also combined) additions of solutes, together with heat treatment, make changes to the precipitate microstructure (i.e. modify types of precipitates, their (dis)order, numbers, sizes and distribution). In this context, detailed knowledge about properties and behaviour of the single solute atoms in supersaturated solid solution can also be important. This concerns their interaction with the Al matrix, that is, with each other and with quenched-in vacancies. Our observations have indicated that precipitation has relation to size of the solute atom as well as to its ability to attract vacancies. We have therefore decided to look more closely into adding Ag and Ge to a lean, industrially relevant Al 6xxx alloy, relating calculated parameters like solute misfit volumes and vacancy bonding energies to experimental observations.

It has recently been found that, if a small amount of Ag is added to an Al-Mg-Si alloy GP-zone formation is enhanced, which correlates with an increased peak hardness of the material [4]. HAADF images showed that Ag occupies Al sites in the matrix as well as in the precipitate, but preferably in the immediate vicinity of the interface [9]. Despite the similar volumes and elemental (fcc) structure of Ag and Al, within the precipitate Ag does copy the behaviour of aluminium, occupying columns between Si (network) columns. In fact, Ag also occupies the otherwise autonomous Si sites. Further on, as the material overages, the β'Ag phase forms [9].

Ge has been added to aluminium alloys in several preceding studies [5] [10] [11]. It is clear that Ge not only passively substitutes Si, but even in very small quantities has a strong refining effect as observed upon heat treatment, yielding a distribution with smaller precipitate needles of higher number density than with only Si. The refinement corresponds with a significant increase in material strength. Although somewhat bigger, Ge clearly occupies Si sites, for example in regions based on the hexagonal column arrangement (Si-

network). That Si and Ge occupy the same atomic sites/columns in a precipitate structure is understandable from their chemical similarity; both are diamond elements. However, in contrast of the apparent seamless substitution in the hexagonal Ge-network, Ge still manages to wreak havoc in most precipitate particles, causing structural disorder even to the point that no repeating unit-cell is detectable in the cross-section plane, or reducing them to assemblies of disordered fractions of known phases. The periodicity along the needles, however, is still intact. By full replacement on the expense of Si, isomorphs of the Mg-Si containing precipitates show up and more order reappears, but the β'' phase completely fails to form [10].

In age hardenable aluminium alloys, the quenched-in vacancy concentration achieved after the cooling from homogenization or solution temperatures is a very important factor for the subsequent nucleation stage of hardening precipitates, partly taking place at room temperature [12] [13]. Vacancies can assemble in clusters and form dislocation loops [13], which can later initiate inhomogeneous and coarse precipitates. The effect gets smaller with more solute and with higher vacancy affinity of the solute elements. It has been demonstrated that vacancy binding energies generally increase with atom size, however not without exception [14]. The elements used in Wolverton's work [14] have vacancy binding energies increasing as Mg, Si, Ag and Ge. A higher solute-vacancy binding corresponds with a higher probability of one or more nearby vacancies.

In this study, we wish to elucidate interesting features recently discovered in the precipitate microstructures from two selected alloys containing Ag or Ge [11]. Structural details observed in the precipitates are discussed in connection with bonding energies and volume misfits acquired through density function theory (DFT) calculations. In this respect, both Ge and Ag are convenient solute elements to investigate because of their high Z-contrast in high angle annular dark-field scanning TEM (HAADF-STEM) experiments. A major part

of the results presented in this work is based on the possibilities of direct determination of atomic columns when using the HAADF-STEM technique, which is affected little by objective lens defocus and specimens thickness compared to high resolution TEM [15] [16].

2 Experimental

2.1. Materials and microscope

Table 1 shows the compositions of the investigated alloys, as measured by inductively coupled plasma optical emission spectroscopy. For a complete description of the heat treatment and TEM specimen preparation, see [11].

Table 1. Alloy composition, effective solute (S_{eff}).

		Si^a	Ge	Mg	Ag	Fe	Mn	S_{eff} [b]
Ag added alloy	wt%	0.35	–	0.30	0.10	0.20	0.03	0.70
	at%	0.34	–	0.33	0.025	0.10	0.015	0.65
Ge added alloy	wt%	0.35	0.10	0.30	–	0.20	0.03	0.70
	at%	0.34	0.04	0.33	–	0.10	0.015	0.66

[a] Effective Si available for precipitation (Si*) is tabulated with an amount 0.05 wt % less [17].

[b] Effective solute S_{eff} = Mg+Si*+Ge+Ag.

The HAADF-STEM images in this work were acquired in a spherical aberration corrected (both probe and image) JEOL ARM200F, equipped with a cold FEG. The operation voltage was 200 kV, the probe size 0.08 nm and the inner collector angle 50 mrad. All precipitates were imaged in a <100>Al direction (here called [001]Al) along the needle/lath extension, which is normal to the cross-section.

Before insertion, the TEM specimens were decontaminated in a Fischione plasma cleaner, model 1020, for 5-7 minutes in O_2/Ar plasma.

2.2. Details for DFT calculations

DFT was applied to find bonding energies between different solute elements and/or vacancies. The lattice parameter used for the calculations is based on the relaxation of an

aluminium supercell consisting of 5x5x5 aluminium unit cells. The unit cell relaxed to 20.20474 Å, i.e. a = 4.04095Å. The interaction energies are estimated from the difference between total energies. All calculations have the same cell size and parameter settings so that any systematic errors should be cancelled out. The bonding energies between two elements are calculated from 1st to 8th nearest neighbour positions. The uncertainty is quite high in the binding energy calculations, between 5 − 10 %, since the total energies of the systems which are subtracted is about -1865 eV. It should be noted that the computed energy differences are quite small and the diffusivity consists of several components.

The Vienna ab initio simulation package (VASP) [18] [19] was used to execute the DFT calculations [20] [21], using the projector augmented wave method (PAW) within the PBE (Perdew-Burke-Ernzerhof) generalized gradient approximation. The plane wave energy cut-off was 400 eV. For all calculations gamma-centred k-points were used, with maximal k-point distances of 0.25 Å^{-1} in each direction. The electronic accuracy for self-consistent loops was set at 10^{-6} eV. The atomic positions were relaxed to a maximum force of 0.001 eV/Å between atoms, using 1st order Methfessel-Paxton for smearing of partial occupation and a smearing factor of 0.2. For accurate energies, a separate calculation was performed using the tetrahedron method with Blöchl correction for the smearing.

Interaction energies are calculated based on equations (1) and (2) below.

$$E_Y = E_{Al499_Y} - \frac{499}{500} E_{Al500} \qquad (1)$$

$$E_{YZ} = E_{Al498\_YZ} - \frac{498}{500} E_{Al500} - E_Y - E_Z \qquad (2)$$

The calculations are based on a cell consisting of 500 Al atoms, Y and Z represents an atom or a vacancy replacing one of the Al atoms in the cell. E_Y and E_Z are the solid solution energies of atom Y and Z respectively. The interaction energy between the two elements Y and Z in the Al cell is calculated by subtracting the solid solution energies of each element from the total electronic energy of the cell. A more detailed explanation of calculating formation energies of structures and solid solution energies of atoms are explained by Ninive et al. in [22].

3 Results

3.1 Interaction energies and volume misfits

Fig. 1 illustrates the interaction energies, as calculated by DFT, between a number of elements including Mg, Ge and Ag in all combinations and the interaction of all three with a vacancy (designated X) in aluminium, as a function of interatomic fcc distances up to two unit distances (8.1 Å). The two first represent the nearest neighbour distance (2.86 Å), and the extent of the unit cell (4.05 Å). The calculations clearly suggest that Ge binds more strongly to vacancies than any of the other alloying elements in this work, while the least favourable arrangement is two vacancies as nearest neighbours.

The calculation of volume misfits of all the relevant elements and vacancies (X) are presented in Fig. 2. The volume of Si is according to Leyson et al. about 13.95 Å3 [23]. Our calculations returned a volume for Si about 13.77Å and that of Ge of about 18.43 Å3. It should be noted that a misfit volume here represents the net expansion or contraction of the entire supercell relative to the substitution of one Al atom by a solute atom or vacancy at 0 K. As the real situation is more complex, a solute atom can be near other solute atoms and vacancies at times. The time spent in the vicinity of each other will depend on the interaction energy at the particular site. A solute-solute or solute-vacancy pair will have more possibilities to deform the surroundings in order to reduce the energy and misfit than a single

solute atom. Also, lattice vibrations at ambient temperature further complicate the picture. This means that the theoretical misfit volumes in Fig. 2 cannot be taken as absolutes. They may be considered as ideal maximum values of isolated solute elements in Al, comparable in a relative sense. The solute-solute or solute-vacancy binding energies give clues about which pairs are likely to reduce the misfit. For example, of the elements in Fig. 1 the bonding between Ge and a vacancy (Ge-X) when on nearest neighbour positions is very low. This means there is a high likelihood of finding a vacancy as nearest neighbour to a Ge atom, something that should tend to relax the surrounding matrix of the pair. The situation is more complex as two or more solutes also attract vacancies and more solute, and as binding energy varies with distance (Fig. 1). An analysis of the information given in Figs. 1 and 2 will be connected to experimental results and presented in the "Discussion" section.
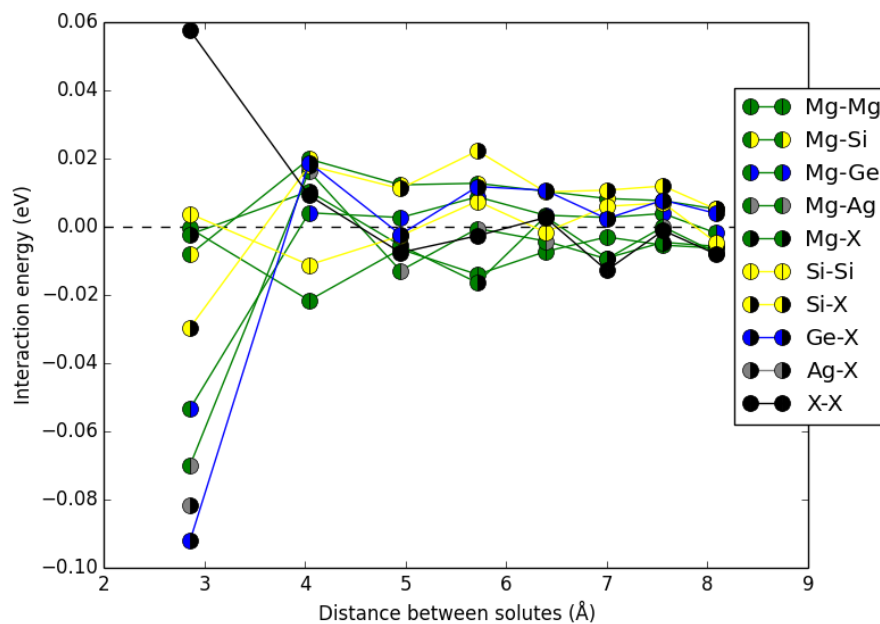

Figure 1. Interaction energies between the alloying elements and/or vacancies (X) in fcc aluminium as a function of separation distance, from 1st to 8th nearest neighbours.
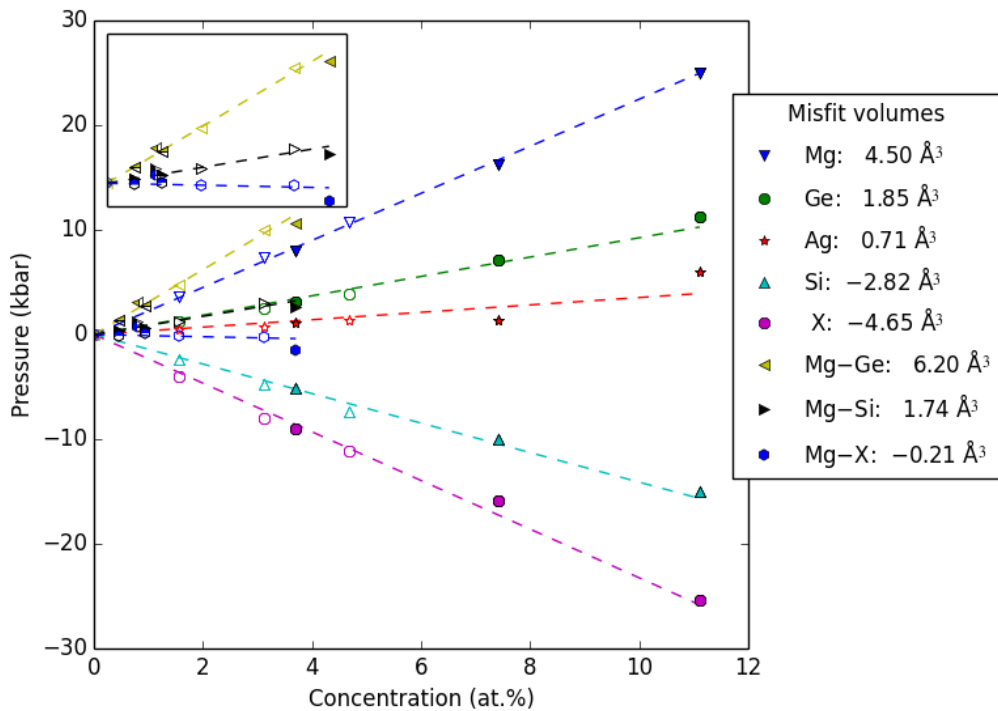
Figure 2. Misfit volumes of the alloying elements and vacancies (X) in fcc aluminium. For single elements in Al: the open symbols indicate calculations based on 3x3x3 primitive cells (27 atoms) and the filled symbols indicate calculations based on 4x4x4 primitive cells (64 atoms). For pairs of elements in Al (insert): open symbols indicate calculations based on 1 pair in 3x3x3, 4x4x4, 5x5x5 and 6x6x6 primitive cells and filled symbols indicate 2 pairs in 4x4x4 and 6x6x6 primitive cells. Dashed lines show linear fits to the data for each element or pair. The misfit volumes are calculated from the slopes as described in [23].

3.2 Detailed overview of precipitate microstructure

Both the Ag - and the Ge - added alloy contained a high number density of the hardening phases, with discernible contents of all added elements. For a complete overview of statistics and comparisons see [11].

Since the hardening phases are all needle/lath shaped along <001> Al, the images show cross-sections with Al and precipitate columns in parallel with this zone axis. In Fig. 3 one representative precipitate (cross section) is given from each alloy. Figs. 4, 5 and 6 have full atomic overlay, based on the Z-contrast from HAADF-STEM, inter-atomic distances and

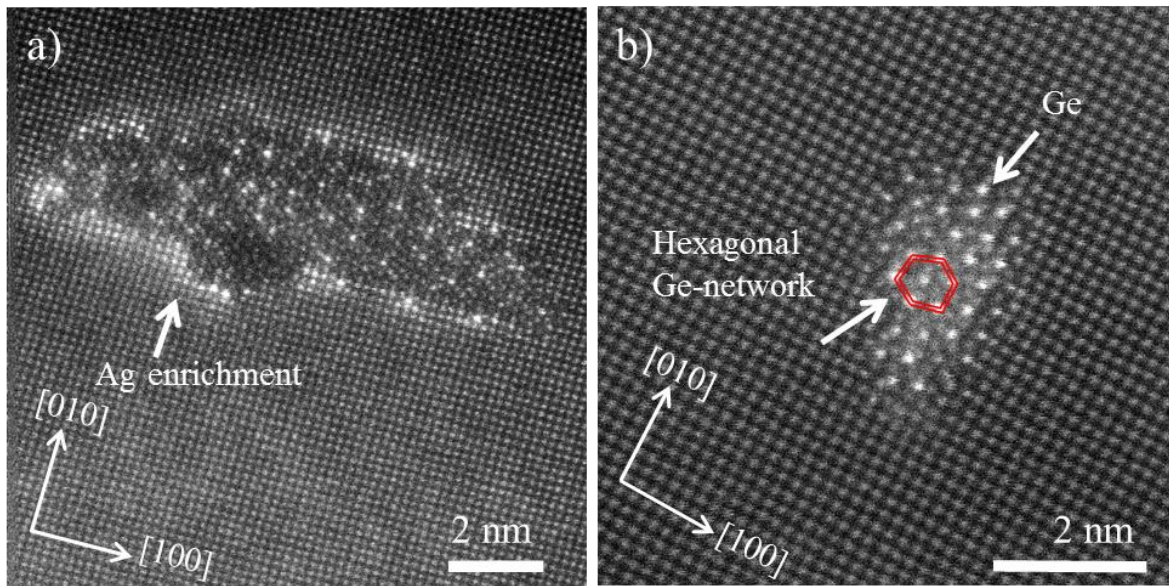local similarities with well-known structures in the Al-Mg-Si/Ge system (see also [6], [9] and [24]).

Figure 3. HAADF STEM raw images of typical precipitate cross-sections from the two alloys illustrating that both Ag and Ge enter and strongly affect atomic structure. a) Large lath-shaped precipitate in Ag added alloy. The high contrast just outside the interface suggests a considerable amount of Ag fully or partly occupying the Al columns. b) A smaller precipitate in the Ge added alloy. The red, double lined hexagon indicates the Ge-network which is extending over the entire precipitate cross section. Very high intensity at these sites verifies the presence of Ge.

3.2.1 Ag added alloy

The silver added alloy contained relatively large precipitates, coarsely distributed in the matrix; see Figs. 3 (a) and 4. The precipitate cross sections had several features in common; in particular, Ag segregation in the matrix near the precipitate interface. Also, fragments of the β'_{Ag} phase appeared frequently together with disordered regions [11]. Interestingly, a new precipitate configuration containing Ag was observed. Similar configurations are normally reported to exist in Cu containing 6xxx alloys and are referred to as Q' or C-plate [6] [25]. In the present study, the "Cu-sites" in the Q'/C - like phase were occupied by Ag. An example of this stacking is given in Fig. 4, where the Q'/C - like local atomic configuration is

10

indicated with yellow, double-lined triangles, hosting an Ag column in its centre. There also seems to be a dislocation progressing along the <010> Al direction through the precipitate, an approximate starting point is indicated by the yellow arrow in Fig. 4.
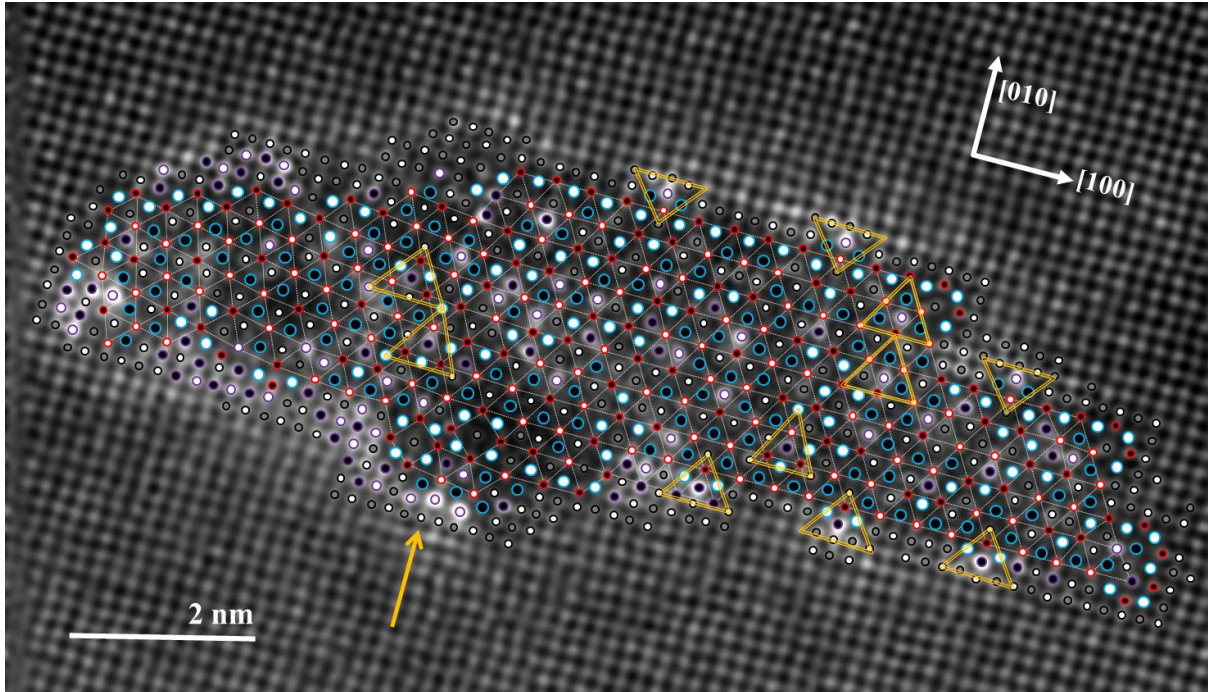

Figure 4. Precipitate cross section in the Ag added alloy with atomic overlay, see Fig. 3 (a) for the original image. The segregation of Ag at the precipitate-matrix interface is evident. The hexagonal Si-network is indicated with dashed, white lines. The Q'/C - like local configurations, where Cu sites are replaced by Ag, are indicated with yellow triangles. For explanation of the symbolic representation of elements, see legend in Table 2.

3.2.2 β'' stacking variations in the Ge added alloy

Version β_2''. Several of the precipitates in the Ge-added alloy demonstrated a second ordering of the "eye-like" β'' molecules, this version of the β'' phase will hereafter be referred to as β_2''. An example of a precipitate cross section incorporating both regular β'', indicated by yellow lines, and the new β_2'', indicated by white dashed lines, is given in Fig. 5 below. The smallest white squares inside the parallelograms show the location of the "vacated columns", also marked by X in Fig. 5 (b).

The β_2'' cell consists of 22 atoms in the projected plane, corresponding to a supercell in the fcc Al lattice of 24 atoms. It should be noted that the common β'' cell consists of 22 atoms, with an Al supercell of 22 atoms. Both β_2'' and normal β'' fulfil the requirements of space group C2/m, however the c-axis of β_2'' lies along <100> Al instead of the usual Al <130> in β''. The ideal composition of β_2'' is similar to that of β'', except for two additional "vacated atomic columns". The composition is given as $Al_6Mg_8D_8X_2$, where D is a mix of Ge and Si, and X here represents a vacant column (see also Fig. 5 (b)). The Si columns in both phases can all be described as "contained by rhombuses" that are pairs of isosceles triangles assembled in different ways. The triangles are the Si network cells of β''. In the supercells on the Al matrix, the triangles are bound by <100> Al and <120> Al directions. In the normal β'' phase, the two triangles are joined on a <120> plane (common leg), as pointed out by red arrows in Fig. 5 (b). In the second β_2'' variant the bases of the triangles meet on a (100) plane, pointed out by yellow arrows in Fig. 5 (b).
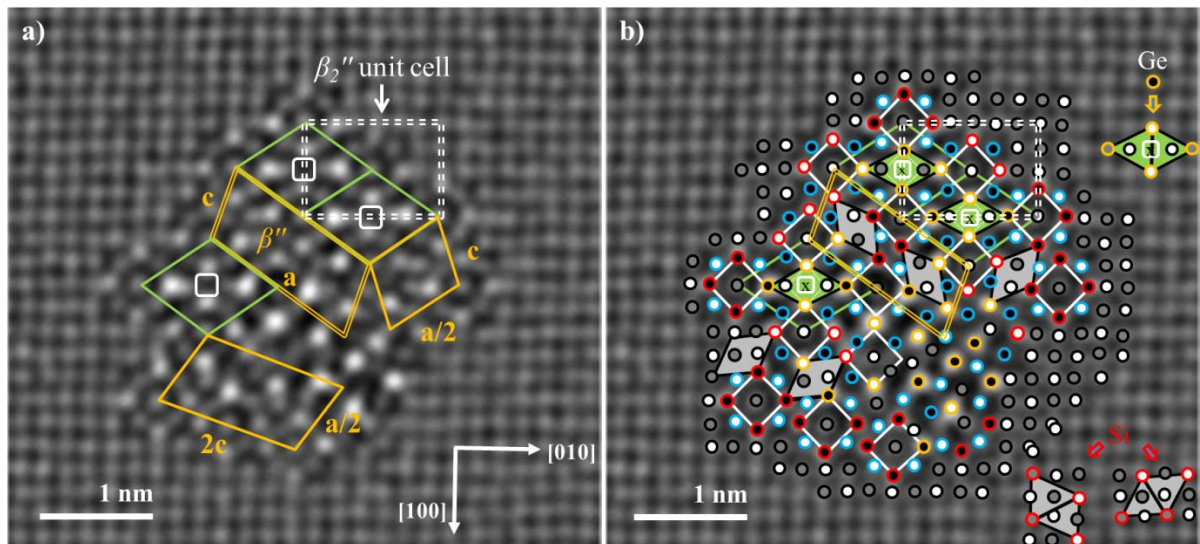

Figure 5. Atomic overlay on the cross section of a precipitate in the Ge-added alloy. Determination of a particular column is based on knowledge of the structures / molecules, intensities in from HAADF-STEM and interatomic distances. See legend in Table 2. In (a) a = <320> a_{Al} = 14.6 Å and c = ½ <130> a_{Al} = 6.40Å. Yellow parallelograms indicate β''

regions and white, green parallelograms indicate β_2'' regions. A β_2'' unit cell is indicated by white dashed lines.

Table 2. Symbolic representation of overlay of elements in Figs. 4, 5, 6 and 7.

Elements / Height	Al	Si	Mg	Ge/Si (D)	Ag/Al
z = 0.000 nm	○	○	○	○	○
z = 0.203 nm	◓	●	●	●	●

Version β_3''. A third version of the β'' phase was discovered in the Ge containing alloy, this phase will hereafter be referred to as β_3''. This stacking variant was not observed as frequently as β_2'', but it occurred occasionally as a fragment in cross sections, combined with β''. A cross section incorporating both the β'' and the β_3'' configuration is shown in Fig. 6. The β_3'' region is marked by white dashed lines. The phase fulfils the requirements of space group C2/m with an ideal composition $Al_{10}Mg_8D_8$. This phase has a cell consisting of 26 atoms; simultaneously its supercell in the Al matrix also covers 26 atoms. The deviation in composition between β_3'' and '$\beta''$and β_2''' is the additional Al columns in the cell.
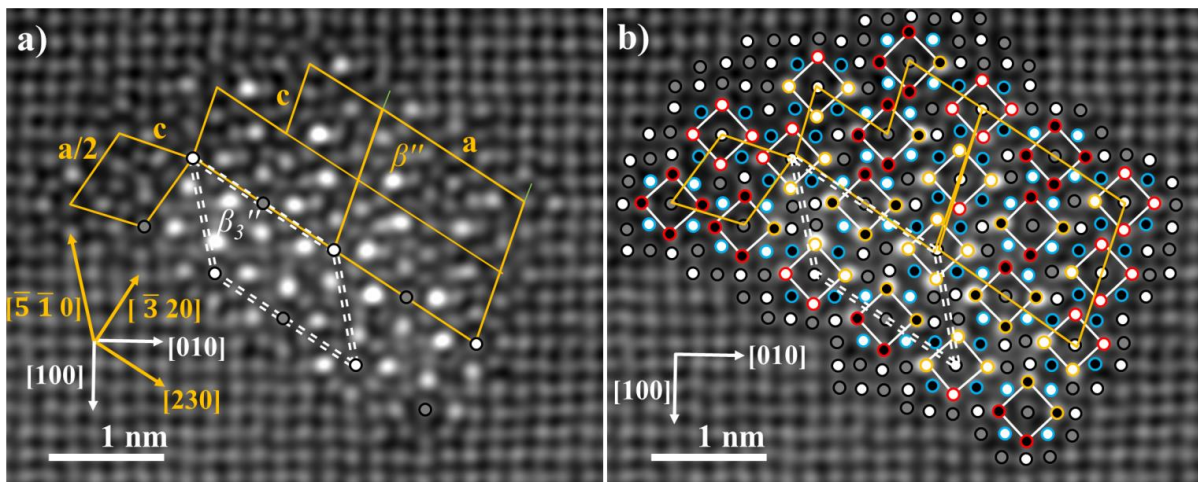

Figure 6. Precipitate exhibiting the β_3'' (white dashed lines) stacking variation of molecules of β''. The regular β'' regions are indicated with yellow solid lines. For explanation of the symbolic representation of elements in (b), see Table 2.

The c-axis of $\beta_3{''}$ lies along <-5-10> Al instead of <130> Al in $\beta{''}$, while the a-axis lies along <230> Al for both variants. The difference between the two could be described as shifting the bottom row of $\beta{''}$-*eyes* with $\approx a/2$ in parallel to the a-axis, consequently the angle between a and c is 135° for $\beta_3{''}$. This shift is present in a Ge-rich area of the cross section; see Fig. 6 (b).

4 Discussion

4.1 Interaction energies and volume misfits

In Fig. 1 Mg-Si nearest neighbour (NN) interaction energy clearly shows that Mg and Si like to be at NN places, that is, it is favourable for these two elements to aggregate pairwise in Al. This result is backed up by the volume misfits in Fig. 2, where a Si atom will contract the Al lattice surrounding it, and Mg will expand it. Combined, Mg and Si seem to lower their misfit in the Al lattice, shown in the insert in Fig. 2. From Fig. 1 and 2 the most favourable Si-Si and Mg-Mg distance in fcc Al is 4.05Å. This would confirm the most common observation for the precipitates: Firstly, that Mg and Si can stay in columns along <001> Al (as they do in parallel with the precipitate extension), and secondly that such columns could alternate along the other <100> Al directions, with atoms as first NNs and columns separated by 2.025Å. As shown in Fig. 1, Mg very weakly attracts vacancies in NN position and then seems to repulse them as 2nd NN. Successively Mg starts to attract vacancies at 3rd and 4th NN positions. The result showing that Mg does not seem to repel vacancies when in 1st NN position corresponds well with the results presented by Wolverton [14]. This indicates that both vacancies and Mg attract the valence electrons less than what Al itself does. From Fig. 2 it is clear that Mg will expand the Al lattice and intuitively this should attract a vacancy. When calculating the volume misfit of Mg and X together, as shown in Fig. 2, we see that the misfit becomes lower than that of Mg or X alone.

Ag should pull strongly on vacancies according to Fig. 1. The precipitate distribution in the Ag-added alloy is however very coarse in comparison, meaning that it does not seem to initiate a high number of nucleation sites, as Ge does. The volume misfit of Ag in Al is however very small. Pure Ag is fcc, as Al itself, and has a relatively high solubility in Al [26]. In the vicinity of a precipitate there would be regions with expansive and contractive strain, meaning slightly more and less space for the solute. We believe this could explain the tendency of Ag accumulating in the Al lattice close to the particle. This also means that for Ag, the most important factor in precipitation should be its volume and its ability to attract vacancies comes in second.

Based on the calculations given in Fig. 1, Ge should pull more strongly on Mg as a NN than Si does. Also, as Ge has a stronger pull on vacancies than Si does, it should be more effective at nucleating clusters. It seems likely that the attraction on both Mg and a vacancy is significant for the ability of Ge to procure favourable nucleation sites for precipitate needles. This result also explains why Ge is mostly localised at the centre of the precipitates, which indicates it is active in the nucleation and growth of the needles from the very beginning. Ge is significantly larger than Si and expands the Al lattice, as opposed to contracting it as Si does, see Fig. 2. It is curious that the Mg-Ge interaction seems favourable at 1st NN places, see Fig. 1, meaning that in the beginning it cannot be the search for minimizing the lattice strain which sets off this aggregation. It is apparent that the charge distribution overcomes the disadvantage of volume misfit as Ge is added to the alloy.

Since the calculations are based on one atom in a (repeated) supercell for all solute elements, this means there is no surface to go to for the solute. Neither the atom nor the vacancy may cross the cell boundary and form a cluster. It should be noted that it is therefore difficult to draw conclusions regarding diffusion based on vacancy binding alone.

4.2 Ag added alloy

The small volume misfit of Ag in Al shown in Fig. 2 is supported by the features seen in Fig. 6, as Ag enriches the Al columns at the interface between the precipitate and the Al matrix. The hexagonal Si-network is present in a major part of this precipitate and is indicated with white triangles. The Si columns are separated by approximately 0.4 nm and the networks height distribution is unique for the precipitate structure [27]. Silver is undoubtedly present inside the precipitate cross section, but it is difficult to establish the occupancy of Ag in the atomic columns, as it is likely they also contain Al [28].

An interesting feature in the precipitate cross section presented in Figs. 3 (a) and 4 is the presence of Q'/C -, or *β'* -like fragments. These fragments are indicated by yellow triangles and were found both at the interface and within the precipitate. Q' and C-plate are documented in Cu-containing alloys and atomistic models have been proposed [6] [25]. In this case, no Cu has been added to the alloy, and the impurity level of Cu is too low for this phase to form. Because of the high Z-contrast in the HAADF-STEM images, the Q'/C sites which usually contain Cu must consequently be occupied by Ag in these precipitates. A model of the new Q'/C - like phase, based on the experimental results and [6] [25] is given in Fig. 7. This shows how it is not only the volume misfits of the solute atoms, Fig. 2, which contribute to the phase formation. Although disposed to occupying Al sites because of similar size, Ag occupies additional sites within the precipitate because of its high interaction energies to other solute elements in Al. From Fig. 1 we see that the interaction energy between Ag and Mg is about – 0.7 eV, which is relatively strong compared to many of the other solute combinations. Based on this result we should expect to also find Ag incorporated in the precipitate structure, interacting with, among other elements, Mg. This is indeed found for both the Q'/C - like phase in Fig. 3, and at Ag sites in Fig. 4. DFT calculations confirmed

that it is energetically favourable for the Q' phase to form in Al, and it does not cost much

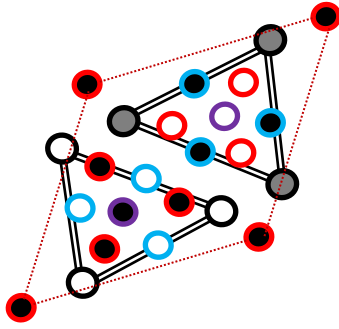energy as the change in cell parameter is small.

Figure 7. Model of the Q'/C - like local configuration, where Ag occupies the site at the centre of the double-lined triangles. Symbols as in Table 2. The model is adapted from the model of the Cu-containing phase in [6].

4.3 β" stacking variations in the Ge added alloy

Models of the three *β"* variants are shown in Fig. 8, with the corresponding lattice parameters

and other characteristics in Table 3. Other compositions are suggested for regular *β"* [1] with

respect to the amount of Al or Mg in each unit cell. For simplicity, we here assume Al

occupies the centre of each "eye" although this position can contain both Al and Mg [1]. The

same applies for the sites often referred to as Si-3 sites since previous works have shown they

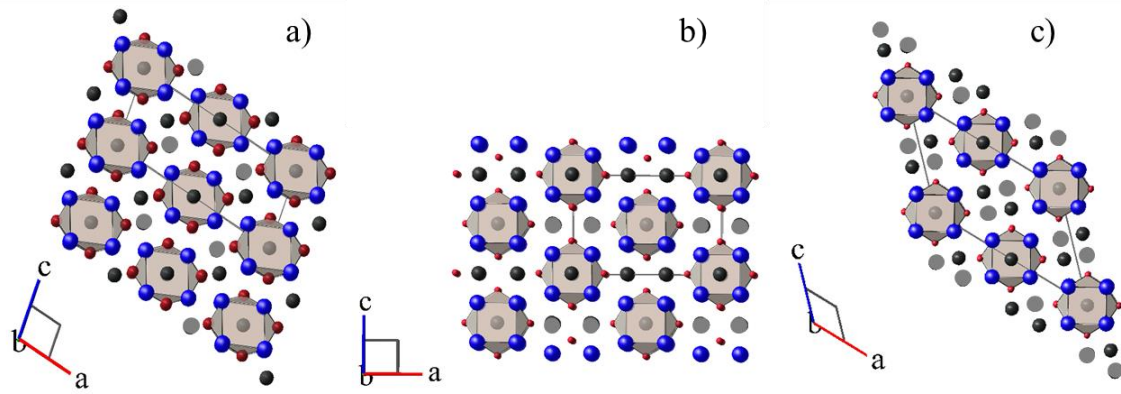are flexible, but usually containing Al in the interface [1]; see Fig. 8.

Figure 8. The three stacking variations of β'', all containing two β'' - *eyes* per unit cell: (a) Normal β'' (b) β_2'' and (c) β_3''. The symbolic representation is as follows: black = Al, blue = Mg and red = Si. The shaded squares and Al atomic columns indicate z = 0.203 nm, while the "non-shaded squares and Al atomic columns" indicate z = 0 nm.

4.3.1 Version β_2''

From Fig. 8 we see that the normal β'' structure has "eyes", each claiming two Al columns (in (a), one Al column on both horizontal sides of the molecule), which account for all Al-columns within the cell. β_2'' contains the same number of eyes and Al columns per molecule, but the alternative ordering means that the unit cell sheds one atomic column relative to the Al super-cell compared to regular β'', see Figs. 5 (a) and (b). The two missing columns in the β_2'' structure means that vacancies must have been absorbed in the process of forming from solutes on fcc positions in the matrix. That β_2'' lacks two columns compared to β'' means that the same amount of atomic columns (same number of molecules) occupy a larger volume in the Al matrix. Using the extracted unit distances and if we assume the expansion only to occur in the precipitate normal plane, the cross-section area increases by 4 %. For a cylinder, this gives 2 % radial expansion. Consequently the tension needed to create an interface dislocation is lowered when the β_2'' stacking occurs. This precipitate type would therefore aid the struggle of keeping added solute to a minimum in lean 6xxx alloys, while at the same time maintaining the material strength.

The β_2'' stacking has been observed in similar Al-Mg-Si alloys, but only as one rhombic unit consisting of four "eyes", hence, it seems Ge is the reason why it becomes energetically favourable for β_2'' to grow more. DFT simulations of precipitates containing both Si and Ge showed that removing the atomic column marked by X in Fig. 5 (b) is indeed energetically favourable for an infinitely long precipitate, and more so for precipitates containing Ge. Moreover, the energy required to form a unit cell of β_2'' is less than that required to form a unit cell of normal β''. DFT revealed it to be advantageous to replace Si with Ge in β_2'', which is exactly what we observe. Another interesting feature of β_2'' is its c-axis lying along <100> Al instead of <130> Al. It has been reported by Bjørge et al. how completely replacing Si by Ge in 6xxx alloys leads to precipitate phases with c-axis lying along <100> Al [10], and no β'' phases form anymore. Normally, the Si-network aligns along <130> Al, however, as Si is replaced by Ge, the hexagonal Ge/Si-network aligns along the <100> Al direction. The β_2'' phase could indeed be an intermediate phase variation in this retrospect, where also here Ge additions cause the c-axis to shift towards the <100> Al direction.

From the NN perspective in Fig. 1 it seems very probable that Mg and Ge would interact closely in the precipitation process, especially since the interaction energy is about five times larger than that between Si and Mg. However, from the misfit volumes in Fig. 2, Mg and Ge has a higher volume misfit as a pair than Mg and Si. When considering the volume of the three stacking variations in Fig. 8, it is clear that β_2'' has a higher volume per "eye" than β''. It seems that the bonding energy between Ge and Mg is high enough to override the relatively large volume misfit of the "eye-like" β'' structure caused by this combination of elements, and we obtain eyes with Ge occupying Si-sites. Ultimately, it appears that these Ge-containing eyes are more likely to form other stacking variations because of higher volume misfit with the Al matrix.

19

4.3.2 Version β3"

The $\beta_3"$ phase has a cell consisting of the same number of atomic columns as its corresponding supercell in Al (26 to 26). $\beta_3"$ does not contain any vacated columns, but more Al columns than both $\beta"$ and $\beta_2"$. As seen in Fig. 8 (c), there are two extra Al-columns per "eye", that is, 8 per two '$\beta"$ *eyes*' instead of 4. More Al inside the precipitate is often associated with a more loosely bound structure, yielding it less efficient as a dislocation impediment. It is possible that we are dealing with a phase normally occurring early in the precipitation sequence, and that upon further heat treatment it would transform into $\beta"$or $\beta_2"$. As shown in Fig. 6 the c-axis lies along <-5 -1 0> Al. This stacking variation leads to the largest unit cell of the three variants presented in Fig. 8 because of the additional Al columns. The supercell in Al has the same number of atomic columns as the unit cell of $\beta_3"$. It could be argued that this phase has a lower Ge content than $\beta_3"$, making the volume misfit with the Al lattice less crucial.

5 Conclusions

Two lean, industrially relevant Al-Mg-Si alloys with Ag or Ge additions were investigated. Precipitate microstructure was examined in detail by HAADF-STEM and the results were corroborated by DFT simulations.

In the Ag added alloy, a version of the Q'/C – local configuration, containing Ag at the Cu - sites was discovered. The low misfit volume of Ag in Al explains why silver often occupies Al columns at the interface of the precipitate surfaces. High binding energies to vacancies and Mg at the same time explain why silver also enters the precipitate structure and sometimes behaves like Cu.

Two new stacking variations of the $\beta"$ phase, referred to as $\beta_2"$ and $\beta_3"$, were discovered in the Ge-added alloy. Germanium's high affinity to vacancies suggests that the element creates more nucleation sites for precipitate needles, thus refining the precipitate

microstructure. β_2'' only appears frequently in the Ge-added alloy. This phase sheds two atomic columns relative to the Al matrix. DFT simulations showed this to be energetically favourable. A high occupancy of Ge together with Mg inside the precipitate structure requires a change in the stacking of β''-*eyes* because of higher volume misfit in Al. The third variant of the β''-phase, β_3'', might be associated with an intermediate phase early in the precipitation sequence because of its higher Al content.

Bibliography

[1] H. S. Hasting, A. G. Frøseth, S. J. Andersen, R. Vissers, J. C. Walmsley, C. D. Marioara, F. Danoix, W. Lefebvre and R. Holmestad, *J. Appl. Phys.,* vol. 106, 2009.

[2] C. D. Marioara, H. Nordmark, S. J. Andersen and R. Holmestad, *J. Mater. Sci.,* vol. 41, pp. 471 - 478, 2006.

[3] R. Vissers, M. A. v. Huis, J. Jansen and C. D. M. S. J. A. H. W. Zandbergen, *Acta Mater. ,* vol. 55, pp. 3815 - 3823, 2007.

[4] M. Kubota, J. F. Nie and B. C. Muddle, "Characterization of Precipitation hardening responce and as-Quenched Microstructures in Al-Mg(-Ag) alloys," *Mater. Trans.,* vol. 45, pp. 3256 - 3263, 2012.

[5] K. Matsuda, S. Ikeno and T. Munekata, "HRTEM Study of Precipitates in Al-Mg-Si and Al-Mg-Ge Alloys," *Mater. Sci. Forum,* Vols. 519 - 521, p. 221, 2006.

[6] T. Saito, C. D. Marioara, S. J. Andersen, W. Lefebvre and R. Holmestad, "Aberration-corrected HAADF-STEM investigations of precipitate structures in Al-Mg-Si alloys with low Cu additions," *Philosophical Magazine,* vol. 94, no. 5, pp. 520 - 531, 2015.

[7] K. Stiller, P. J. Warren, V. Hansen, J. Angenete and J. Gjønnes, "Investigation of precipitation in an Al-Zn-Mg alloy after two step ageing treatment at 100C and 150C," *Materials Science and*

Engineering: A, vol. 270, no. 1, pp. 55 - 63, 1999.

[8] F. W. Gayle and J. B. V. Sande, "Composite precipitates in an AlLiZr alloy," *Scripta Metallurgica,* vol. 18, no. 5, pp. 473 - 478, 1984.

[9] C. D. Marioara, J. Nakamura, K. Matsuda, S. J. Andersen, R. Holmestad, T. Sato, T. Kawabata and S. Ikeno, *Phil. Mag.,* vol. 92, pp. 1149 - 1158, 2012.

[10] R. Bjørge, C. D. Marioara, S. J. Andersen and R. Holmestad, *Metal. Mater. Trans. A,* vol. 41, p. 1907, 2010.

[11] E. A. Mørtsell, C. D. Marioara, S. J. Andersen, J. Røyset, O. Reiso and R. Holmestad, *Metallurgical and Materials Transactions A,* vol. 46, no. 9, pp. 4369 - 4379, 2015.

[12] L. A. Westfall, "An investigation of nano-voids in quenched aluminium by small-angle x-ray scattering," Queen's University, Kingston, Ontario, Canada, 2008.

[13] V. Gavini, K. Bhattacharya and M. Ortiz, "Vacancy clustering and prismatic dislocation loop formation in aluminium," *Phys. Rev. B,* vol. 76, p. 180101, 2007.

[14] C. Wolverton, *Acta Mater. ,* vol. 55, pp. 5867 - 5872, 2007.

[15] T. Yamazaki, M. Kawasaki, K. Watanabe, I. Hashimoto and M. Shiojiri, *Ultramicroscopy,* vol. 92, p. 181, 2002.

[16] P. D. Nellist and S. J. Pennycook, *Ultramicroscopy,* vol. 78, p. 111, 1999.

[17] U. Tundal, O.Reiso, E. Hoff, R. Dickson and C. Devadas, in *Proc. 10th International Aluminum Extrusion Technology Seminar*, Miami, 2012.

[18] G. Kresse and J. Hafner, "Ab initio molecular dynamics for liquid metals," *Phys. Rev. B,* vol. 32, pp. R558 - R561, 1993.

[19] G. Kresse and J. Furthmüller, "Efficiency of ab initio total energy calculations for metals and semiconductors using a plane wave basis set.," *Comput. Mater. Sci.,* vol. 6, pp. 15 - 50, 1996.

[20] P. Hohenberg and W. Kohn, "Inhomogeneous Electron Gas," *Phys. Rev.,* vol. 136, pp. B864 - B871, 1964.

[21] K. W. and S. L. J., "Self-Consistent Equations Including Exchange and Correlation Effects," *Phys. Rev.,* vol. 140, pp. A1133 - A1138, 1965.

[22] P. H. Ninive, A. Strandlie, S. Gulbrandsen-Dahl, W. Lefebvre, C. D. Marioara, S. J. Andersen, J. Friis, R. Holmestad and O. M. Løvvik, "Detailed atomistic insight itno the beta" phase in Al-Mg-Si alloys," *Acta Materialia,* vol. 69, pp. 126 - 134, 2014.

[23] G. P. M. Leyson, L. G. Hector and W. A. Curtin, "Solute strengthening from first principles and application to aluminum alloys," *Acta Mat.,* vol. 60, pp. 3873 - 3884, 2012.

[24] M. Torsæter, F. J. H. Ehlers, C. D. Marioara, S. J. Andersen and R. Holmestad, "Applying precipitate-host lattice coherency for compositional determination of precipitates in Al-Mg-Si-Cu alloys," *Philosophical Magazine,* vol. 92, no. 31, pp. 3833 - 3856, 2012.

[25] C. D. Marioara, S. J. Andersen, T. N. Stene, H. Hasting, J. Walmsley, A. T. J. V. Helvoort and R. Holmestad, *Philosophical Magazine,* vol. 87, p. 3385, 2007.

[26] A. J. McAlister, "The Ag-Al (Silver - Aluminum) system," *Bulletin of Alloy Phase Diagrams,* vol. 8, no. 6, pp. 526 - 533, 1987.

[27] F. J. H. Ehlers, S. Wenner, S. J. Andersen, C. D. Marioara, W. Lefebvre, C. B. Boothroyd and R. Holmestad, "Phase stabilization principle and precipitate-host lattice influences for Al-Mg-Si-Cu alloy precipitates," *J Mater Sci,* vol. 49, pp. 6413 - 6426, 2014.

[28] E. A. Mørtsell, S. Wenner, P. Longo, S. J. Andersen, C. D. Marioara and R. Holmestad, "Elemental electron energy loss mapping of a precipitate in a multi-component aluminium alloy," *Micron,* April 2016.